Observing strongly interacting vector boson systems at the CERN Large Hadron Collider

C. Englert,[1] B. Jäger,[2,3] M. Worek,[1,4] and D. Zeppenfeld[1]

[1]*ITP, Universität Karlsruhe, 76128 Karlsruhe, Germany*

[2]*Institut für Theoretische Physik und Astrophysik, Universität Würzburg, 97074 Würzburg, Germany*

[3]*KEK Theory Division, 305-0801 Tsukuba, Japan*

[4]*Institute of Physics, University of Silesia, 40-007 Katowice, Poland*

(Received 2 November 2008; published 28 August 2009)

We explore the potential of the CERN Large Hadron Collider to access a strongly interacting electroweak symmetry breaking sector via weak boson scattering with W^+W^-jj, $ZZjj$, and $W^\pm Zjj$ final states. As examples of models with scalar or vector resonances we concentrate on a scenario with a heavy Higgs boson and on a warped Higgsless Kaluza-Klein model of narrow spin-one resonances. The signal and the most prominent background processes are evaluated using exact tree-level matrix elements including full off-shell and finite width effects for final states with two tagging jets and four leptons. Using double forward jet-tagging techniques, we derive dedicated cuts on the observable jets and charged leptons to suppress standard model backgrounds. We demonstrate that the LHC has substantial sensitivity to strong interactions in the electroweak symmetry breaking sector.

DOI: 10.1103/PhysRevD.80.035027 PACS numbers: 11.15.Ex, 11.80.La, 12.15.−y, 12.60.Nz

I. INTRODUCTION

An essential goal of the CERN Large Hadron Collider (LHC) [1,2] is gaining information on the mechanism which breaks the electroweak (EW) symmetry. Particularly promising means for probing electroweak symmetry breaking are provided by weak boson scattering reactions, $VV \to VV$ (with V denoting a $W^\pm$ or Z boson). The respective scattering amplitudes for longitudinally polarized vector bosons grow with energy, thus violating unitarity beyond about 1 TeV [3–5], when Feynman graphs with vector bosons only are considered. Taming of this unphysical growth can be attained by a standard model (SM) Higgs boson [6–8], but also strong couplings among the gauge bosons may serve to cure the growth of the VV scattering amplitudes at high energies [9–11]. Various models have been suggested in which the unitarization of these scattering amplitudes is realized by new excitations stemming from the compactification of extra-dimensional theories [12–14], based on the ideas of [15]. At the LHC, weak boson scattering can be accessed via vector boson fusion (VBF) reactions, where the quarks emerging from the scattering protons emit t-channel weak bosons which in turn scatter off each other. A Higgs boson as predicted by the SM would manifest itself as a relatively low mass resonance in this reaction, but the VBF cross section would remain perturbatively small at di-boson masses well above the Higgs boson mass. In the case of strongly interacting gauge bosons, the production rate of longitudinally polarized gauge boson pairs V_LV_L is significantly enhanced at $m_{VV} \approx 1$ TeV, before unitarizing effects reduce the scattering amplitudes.

Signal events from strong V_LV_L scattering processes via $qq \to qqVV$ in VBF exhibit unique signatures. The decay leptons of the gauge bosons emerge almost back-to-back in the central region of the detector with large transverse momenta and high invariant mass. The scattered quarks give rise to highly energetic jets of relatively low transverse momenta in the forward and backward regions. Because of the colorless weak boson exchange, the hadronic jet activity in the central regions is very low. These distinctive features can be exploited to efficiently reduce background processes with respect to the V_LV_L signals.

The goal of this study is to refine the analyses of Refs. [16–19] for strongly interacting electroweak symmetry breaking. Instead of using single forward jet tagging, as in these early analyses, we will consider the boost invariant double forward jet-tagging techniques which have proven highly efficient for the search of a light Higgs boson in VBF [20–23]. These more efficient jet-tagging techniques will allow us to relax the cuts on the VV decay leptons as compared to Ref. [19]. A second refinement is in the level of signal and background simulation. We use parton-level calculations for the processes $pp \to VVjj$ at $\mathcal{O}(\alpha^6)$ and $\mathcal{O}(\alpha^4\alpha_s^2)$ including leptonic decays of the weak bosons, as well as a simulation of the $t\bar{t}$, $t\bar{t}j$, and $t\bar{t}jj$ background processes at $\mathcal{O}(\alpha^4\alpha_s^2)$, $\mathcal{O}(\alpha^4\alpha_s^3)$, and $\mathcal{O}(\alpha^4\alpha_s^4)$, respectively. This corresponds to tree-level amplitudes for all processes and includes full off-shell effects for top-quark decays $t \to Wb$ and for the leptonic decays of the weak bosons in all signal and background processes. While comparable accuracy of the simulations has been discussed in the literature for individual reactions (see, e.g., Refs. [24–26]), an analysis of VBF signal and background processes with full leptonic decay correlations and off-shell effects is new. Phenomenological studies for other production modes of extra vector resonances have recently been performed in [27–31].

For the signal processes, we consider two different models for the strongly interacting electroweak symmetry breaking. We model unitarity conservation with a heavy

and broad standard model scalar Higgs resonance, which we take as a prototype for models with strong VV scattering. As a model with extra vector resonances, we adapt a warped Higgsless scenario where unitarity violation is postponed by the exchange of additional spin-one Kaluza-Klein (KK) resonances. On the basis of these two distinct examples, we show that independent of whether the unitarity-restoring interactions are of a scalar or vector nature, our set of cuts and signal processes provides a clear signature with a large signal-to-background ratio.

Our paper is organized as follows: Section II outlines the theoretical setup for the two signal scenarios which we consider. The framework of the phenomenological analysis is described in Sec. III and here we also give details on the Monte Carlo calculation of the various signal and background processes. In Sec. IV we present the numerical results for expected cross sections at the LHC. Section V contains our conclusions.

II. THEORETICAL SETUP

Strongly coupled theories have a long history as extensions of the standard model [32–34]. In these models the additional degrees of freedom, needed to unitarize longitudinal gauge boson scattering, originate from a strongly interacting sector that produces scalar and vectorial composites. While electroweak symmetry breaking is stabilized at the electroweak scale, the compositness scale is in principle a free parameter. The unitarizing mass spectrum can be rather heavy and broad, due to strong couplings in the composite sector. As such models are intrinsically nonperturbative; there are large theoretical uncertainties on the theory's parameters that can only roughly be estimated by naive dimensional analysis [35]. This poses a huge challenge for modelling LHC phenomenology. For this reason we use unitarity of longitudinal VV scattering at the TeV scale as a key ingredient to model the strongly interacting sector, focusing on two distinct scenarios: In the first one, we adapt a heavy and broad scalar resonance, while in the second one, longitudinal gauge boson scattering is unitarized by vectorial resonances in the warped Higgsless model of Refs. [12,13].

A. Scalar resonance

Within the SM, unitarization of longitudinal VV scattering is achieved by adding the contributions of a scalar resonance of zero isospin, the Higgs boson, to the gauge boson exchange graphs which are mandated by the gauge symmetry. Working within the SM, precision data, in particular, the results of LEP and the Stanford Linear Collider (SLC) on various four-fermion processes combined with the direct Higgs search at LEP, constrain the mass of the SM Higgs boson to lie inside the 100–200 GeV region [36,37]. Strictly within the SM, a heavy scalar resonance, with a mass of order 1 TeV, is ruled out as a model for unitarized weak boson scattering.

These SM Higgs boson mass bounds might be misleading, however, if other new physics contributions to four-fermion amplitudes (partially) cancel the virtual contributions of a heavy Higgs boson to the S and T parameters [38–41], thus mitigating the constraints from precision experiments. Since the precision observables, with their strong focus on four-fermion amplitudes, and weak boson scattering amplitudes are independent entities in sufficiently general models of new physics, we ignore the constraints from precision data in the following and consider, as a phenomenological model, unitarization of weak boson scattering by a scalar resonance with quantum numbers and couplings identical to a heavy SM Higgs boson. We include s-, t-, and/or u-channel exchange of this resonance and use $m_H = 1$ TeV and a fixed width $\Gamma_H = 0.5$ TeV as a toy model for demonstration purposes. This fixed width is included for timelike and spacelike propagators, in analogy to the complex mass scheme for the gauge boson propagators. More general model parameters of a heavy scalar resonance can easily be implemented in the VBFNLO program [42] which we use for all signal simulations.

B. Vectorial resonances

As an example of unitarization with vectorial resonances we consider a phenomenological version of the warped Higgsless model of Refs. [43,44]. Using the AdS/CFT correspondence [45–47], the warped Higgsless scenario can be considered as a particular type of a strongly interacting walking technicolor theory [46], yet being calculable by perturbative means from a bulk-gauged effective theory defined on a slice of a five-dimensional anti–de Sitter space. In these scenarios the growth of the amplitude in longitudinal gauge boson scattering is tamed by the exchange of heavy spin-one Kaluza-Klein excitations, $W_k^{\pm}$ and Z_k. Demanding sum rules for the quartic and triple vector boson couplings [27,48],

$$g_{W_1W_1W_1W_1} = \sum_{k\geq 0} g^2_{W_1W_1Z_k}, \tag{1}$$

$$4m^2_{W_1} g_{W_1W_1W_1W_1} = 3\sum_{k\geq 1} m^2_{Z_k} g^2_{W_1W_1Z_k}, \tag{2}$$

$$g_{W_1W_1Z_1Z_1} = \sum_{k\geq 1} g^2_{W_kW_1Z_1}, \tag{3}$$

$$2(m^2_{Z_1} + m^2_{W_1}) g_{W_1W_1Z_1Z_1} = \sum_{k\geq 1} g^2_{W_kW_1Z_1}\left(3m^2_{W_k} - \frac{(m^2_{Z_1} - m^2_{W_1})^2}{m^2_{W_k}}\right), \tag{4}$$

results in good high energy behavior of the V_LV_L scattering amplitude. In (1)–(4), k labels the Kaluza-Klein states, and $k = 0, 1$ identifies the massless and massive gauge bosons of the SM, respectively. We focus on a scenario where the

new additional massive vector bosons have vanishing couplings to SM fermions, and include states up to W_4 and Z_6.

Higgsless symmetry breaking has already been studied in various realizations [12–14,27–31,49–51]. In this paper we do not attempt to construct a realistic model of Higgsless symmetry breaking, but we solely use the quoted sum rules as a phenomenological paradigm of unitarization with isovectorial resonances. For a more detailed discussion on the implementation of the sum rules and the KK mass spectrum, we refer the reader to a separate publication [44].

III. FRAMEWORK OF THE ANALYSIS

Throughout this study, we consider vector boson pair production in association with two tagging jets, $pp \to VVjj$, with subsequent leptonic decays of the gauge bosons in proton-proton collisions at the LHC with a center-of-mass energy of 14 TeV. If strong interactions among longitudinally polarized vector bosons are realized in nature, $V_L V_L \to V_L V_L$ scattering is expected to be enhanced at large invariant mass. In contrast, the scattering of transversely polarized gauge bosons V_T is dominated by the same weak gauge interactions as in the SM light Higgs boson scenario and, thus, remains perturbative throughout the entire VV invariant mass range. The $V_T V_T \to V_T V_T$ and $V_L V_T \to V_L V_T$ contributions to vector boson scattering must be considered as an irreducible background to the signature of strong gauge boson interactions, which we wish to isolate. We thus define the VBF "signal" in EW $pp \to VVjj$ production as the enhancement of the cross section over the SM prediction with a light Higgs boson. In the heavy Higgs boson scenario this is

$$\sigma_S \equiv \sigma_{\mathrm{SM}}(m_H = 1\ \mathrm{TeV}) - \sigma_{\mathrm{SM}}(m_H = 100\ \mathrm{GeV}). \quad (5)$$

As an alternative realization of electroweak symmetry breaking we consider the warped Higgsless Kaluza-Klein model described in Sec. II B. In this context we define

$$\sigma_S \equiv \sigma_{\mathrm{KK}} - \sigma_{\mathrm{SM}}(m_H = 100\ \mathrm{GeV}). \quad (6)$$

Backgrounds arise from QCD-induced and nonresonant EW reactions with the same final-state configuration as the signal, at $\mathcal{O}(\alpha^4\alpha_s^2)$ and $\mathcal{O}(\alpha^6)$, respectively. For the W^+W^-jj channel, the production processes $t\bar{t}$, $t\bar{t}j$, and $t\bar{t}jj$ at $\mathcal{O}(\alpha^4\alpha_s^2)$, $\mathcal{O}(\alpha^4\alpha_s^3)$, and $\mathcal{O}(\alpha^4\alpha_s^4)$, respectively, have to be considered as copious background sources also. Via their decay chains, the $t\bar{t}$ pairs give rise to the same combination of charged leptons in the final state as the VBF signal process.

Since the principle subject of this study is the investigation of strongly interacting gauge boson systems, we do not consider signal processes deriving from Yukawa couplings of the Higgs boson to fermions, such as gluon-induced Hjj production.

A. Details of the calculation

The calculation of cross sections and kinematic distributions for all signal and background processes introduced above is performed with two independent computer programs featuring full tree-level matrix elements:

(i) Results for all but Kaluza-Klein signal reactions are generated with HELAC-PHEGAS, a completely automatic Monte Carlo event generator [52–56], which calculates matrix elements through Dyson-Schwinger off-shell recursive equations. The package provides events for arbitrary parton-level processes in the most recent Les Houches Accord format [57] and has successfully been tested for scattering reactions at a future linear collider [58] and at the LHC [59].

(ii) The EW VBF and Kaluza-Klein signal and background processes are tackled with the tree-level version of VBFNLO [42], a parton-level Monte Carlo program for VBF-type reactions. For the QCD $VVjj$ processes, we implemented MADGRAPH-generated amplitudes [60,61] into the framework of VBFNLO. Results for the $t\bar{t}$, $t\bar{t}j$, and $t\bar{t}jj$ reactions are generated with the codes of Ref. [24].

Making sure that the different programs yield the same results provides an excellent check of our calculation. In particular, HELAC-PHEGAS agrees at least at the level of 1% with the top backgrounds of Ref. [24], and even better with the MADGRAPH-type implementation of the QCD $VVjj$ backgrounds in VBFNLO, irrespective of the cuts applied.

For our numerical studies we use the CTEQ6L1 parton distribution functions [62,63] at leading order (LO) with $\alpha_s(M_Z) = 0.130$. We have chosen $M_Z = 91.188$ GeV, $M_W = 80.423$ GeV, and $G_F = 1.166 \times 10^{-5}/\ \mathrm{GeV}^2$ as electroweak input parameters. The other parameters, α and $\sin^2\theta_W$, are computed thereof via LO EW relations. The masses of the top and bottom quarks are set to $m_t = 172.5$ GeV and $m_b = 4.4$ GeV, respectively. Contributions from b and t quarks in the initial state are neglected throughout. In HELAC-PHEGAS, finite width effects in massive vector boson and top-quark propagators are taken into account by the complex mass scheme of Refs. [64–66]. Both, in VBFNLO and in the code of Ref. [24], unstable particles are treated via modified versions [67,68] of the complex mass scheme. Spin and color correlations of the final-state particles are taken into account without any approximations. Final-state partons are recombined into jets according to the k_T algorithm [69–71] with resolution parameter 0.7. In the following, we outline the process-specific settings of our analysis.

1. EW $VVjj$ production

EW $VVjj$ production mainly proceeds via the fusion of weak bosons in the t channel in quark-(anti)quark scatter-

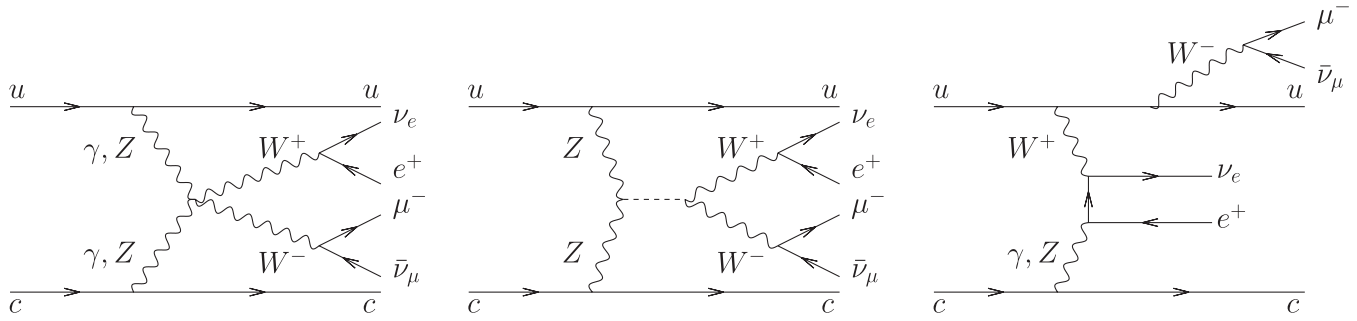

FIG. 1. Examples of Feynman-graph topologies contributing to EW W^+W^-jj production at $\mathcal{O}(\alpha^6)$.

ing processes like $qq' \to qq'VV$. In experiment, however, leptons rather than vector bosons are identified. We therefore focus on the reactions

$$\begin{aligned} &pp \to \ell^+\nu_\ell\ell'^-\bar{\nu}_{\ell'}jj, \qquad pp \to \ell^+\ell^-\ell'^+\ell'^-jj, \\ &pp \to \ell^+\ell^-\nu_{\ell'}\bar{\nu}_{\ell'}jj, \qquad pp \to \ell^+\nu_\ell\ell'^+\ell'^-jj, \\ &\qquad\qquad pp \to \ell^-\bar{\nu}_\ell\ell'^+\ell'^-jj, \end{aligned} \tag{7}$$

at $\mathcal{O}(\alpha^6)$, which include the resonant $VVjj$ production processes with subsequent leptonic decays and additional single- and nonresonant diagrams; see Fig. 1. We only simulate decays of the weak bosons to different lepton generations, e.g. $W^+W^- \to e^+\nu_e\mu^-\bar{\nu}_\mu$. Same-generation lepton interference effects as occurring in $W^+W^- \to e^+\nu_e e^-\bar{\nu}_e$ are neglected for all production channels. However, we adjust counting factors to correspond to the production of all combinations of charged leptons of the first two generations. In the case of $Z \to \nu_\ell\bar{\nu}_\ell$ we sum over three neutrino generations, i.e. $\nu_\ell\bar{\nu}_\ell = \nu_e\bar{\nu}_e,\ \nu_\mu\bar{\nu}_\mu$, and $\nu_\tau\bar{\nu}_\tau$. For brevity, we will refer to these reactions as EW W^+W^-jj, $ZZjj \to 4\ell jj$, $ZZjj \to 2\ell 2\nu jj$, W^+Zjj, and W^-Zjj production, respectively, even though we are always considering leptonic final states.

As discussed in Refs. [72–75], compared to the dominant t-channel configurations, contributions from s-channel electroweak boson exchange and identical fermion effects are negligible in the phase-space regions where $VVjj$ production is observed experimentally. They are therefore disregarded for our analysis. In Ref. [74] it has been demonstrated that next-to-leading order (NLO) QCD effects can be well approximated also in distributions by a proper choice of the factorization scale, μ_F, in the LO calculation: for each fermion line choose the momentum transfer Q between the respective initial- and final-state quarks. We therefore set $\mu_F = Q$ for all EW $VVjj$ processes.

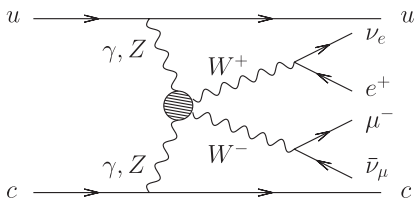

FIG. 2. Modified weak boson fusion topology. The shaded area contains different Kaluza-Klein intermediate states.

2. *Higgsless* $VVjj$ *production*

The implementation of the Kaluza-Klein scenario described in Sec. II B into the VBFNLO framework is described in detail in Refs. [43,44]. The leptonic tensors for subamplitudes such as $ZZ \to e^+\nu_e\mu^-\bar{\nu}_\mu$ in Fig. 2 have been extended by the different Kaluza-Klein intermediate states. We discard interactions of non-SM Kaluza-Klein gauge bosons with the light SM fermions. The coupling of the Kaluza-Klein W_k and Z_k to the W_1 and Z_1 steeply drops off with the Kaluza-Klein index k. For $k \geq 3$, contributions of Kaluza-Klein excitations to cross sections and distributions are tiny [44]. In our studies we include all Kaluza-Klein states up to W_4 and Z_6 with the masses and widths as given in Table I.

Gauge boson pair production in the presence of Kaluza-Klein excitations proceeds analogously to Higgs-mediated $VVjj$ production. In order to absorb the dominant NLO-QCD effects we therefore use the same factorization scales as for EW $VVjj$ production, i.e. $\mu_F = Q$ [43,44].

TABLE I. Masses and widths of the Kaluza-Klein resonances used in the simulation. The spectrum corresponds to a Planck brane localization $R = 9.75 \times 10^{-9}$ GeV^{-1}.

Particle	m (GeV)	Γ (GeV)
W_2	700	13.7
Z_2	695	8.7
Z_3	718	6.4
W_3	1106	31.0
Z_4	1112	26.5
W_4	1585	56.5
Z_5	1580	31.7
Z_6	1605	24.1

3. QCD $VVjj$ production

QCD-induced $VVjj$ production calculated at order $\mathcal{O}(\alpha^2\alpha_s^2)$ includes the production processes

$$qq \to qqVV, \qquad qg \to qgVV, \tag{8}$$

with subsequent leptonic decays, and all crossing-related reactions.

For these processes we use $\mu_F = \min(p_{Tj_1}, p_{Tj_2})$. The renormalization scale is chosen such that the strong coupling factor takes the form $\alpha_s^2 = \alpha_s(p_{Tj_1}) \cdot \alpha_s(p_{Tj_2})$, i.e. the transverse momentum of each parton is taken as the relevant scale for its production.

4. $t\bar{t}$ + jets production

Because of the large top-quark production rate at the LHC and because the branching ratio $B(t \to Wb)$ is essentially 100%, $t\bar{t}$ + jets processes constitute a major background to EW W^+W^-jj production. We consider the reactions $pp \to t\bar{t}$, $t\bar{t}j$, and $t\bar{t}jj$ which include full off-shell and finite width top and W effects and take into account the double-resonant, single-resonant, and nonresonant contributions at order $\mathcal{O}(\alpha^2\alpha_s^2)$, $\mathcal{O}(\alpha^2\alpha_s^3)$, and $\mathcal{O}(\alpha^2\alpha_s^4)$, respectively. To avoid double counting, the top-quark backgrounds are separated into three categories, depending on whether two, one, or zero $b(\bar{b})$ quarks are identified as tagging jets and are referred to as $t\bar{t}$, $t\bar{t}j$, and $t\bar{t}jj$ background, respectively. When combining these processes, we proceed as follows: For $t\bar{t}jj$ production both tagging jets are required to arise from massless partons, while in the $t\bar{t}j$ case exactly one tagging jet is allowed to emerge from a b or $\bar{b}$ quark. For $t\bar{t}$ production both tagging jets stem from b quarks [22,23]. When presenting cross sections and kinematic distributions, the three $t\bar{t}$ + jets backgrounds are combined for clarity even though their individual distributions are slightly different.

In all cases, the factorization scale is chosen as $\mu_F = \min(m_{T_i})$ of the top quarks and additional jets, where each m_{T_i} is given by the transverse momentum and mass of the respective entity i as

$$m_{T_i} = \sqrt{p_{T_i}^2 + m_i^2}. \tag{9}$$

The overall strong coupling factors for the $t\bar{t}$ + $n$jets cross section are calculated as $(\alpha_s)^{n+2} = \prod_{i=1}^{n+2} \alpha_s(m_{T_i})$.

B. Selection cuts

In order to suppress the backgrounds with respect to the signal processes, the design of dedicated selection cuts is essential. For our analysis we have developed various sets of cuts, which are given as follows:

(I) Inclusive cuts: Basic selection cuts need to be introduced to render our calculation of the production cross sections of all signal and background processes finite. This is achieved by identifying all final-state massless partons with high transverse momentum jets. The two jets of largest transverse momentum are called "tagging jets" and are required to carry

$$p_{Tj}^{\text{tag}} > 30 \text{ GeV}. \tag{10}$$

All jets need to lie in the rapidity range accessible to the detector,

$$|\eta_j| < 4.5, \tag{11}$$

and are supposed to be well separated,

$$\Delta R_{jj} = \sqrt{(\eta_{j_1} - \eta_{j_2})^2 + (\phi_{j_1} - \phi_{j_2})^2} > 0.7, \tag{12}$$

with η_j denoting the jet rapidity and ΔR_{jj} the separation of any pair of jets in the rapidity-azimuthal angle plane. For all $VVjj$ production processes, the tagging jets are identified with the massless final-state partons of the reaction. For the $t\bar{t}$ + jets backgrounds, the tagging jets can stem from a massless quark or gluon, or from the decay products of the top quarks.

In order to ensure well-observable isolated charged leptons in the central-rapidity region, we require

$$p_{T\ell} > 20 \text{ GeV}, \qquad |\eta_\ell| < 2.5, \qquad \Delta R_{\ell j} > 0.4, \tag{13}$$

where $\Delta R_{\ell j}$ stands for the separation of a charged lepton from any jet. Since any b quark close to a charged lepton is very likely to also spoil lepton isolation, we require $\Delta R_{\ell b} > 0.4$ even if the b quark is too soft to qualify as a jet. Finally, a cut on the invariant mass $m_{\ell\ell}$ of two charged leptons of the same flavor is applied to avoid virtual photon singularities stemming from quasicollinear $\gamma^* \to \ell^+\ell^-$ decays,

$$m_{\ell\ell} > 15 \text{ GeV}. \tag{14}$$

(II) VBF cuts: VBF events are characterized by two tagging jets in the far forward and backward regions of the detector, while the leptonic decay products of the vector bosons are typically located in the central-rapidity range between the jets. To favor such configurations, we demand that the charged leptons fall between the tagging jets,

$$\eta_{j,\min}^{\text{tag}} < \eta_\ell < \eta_{j,\max}^{\text{tag}}, \tag{15}$$

which are well separated in rapidity,

$$\Delta\eta_{jj} = |\eta_{j_1}^{\text{tag}} - \eta_{j_2}^{\text{tag}}| > 4, \tag{16}$$

and occupy opposite detector hemispheres,

$$\eta_{j_1}^{\text{tag}} \times \eta_{j_2}^{\text{tag}} < 0. \tag{17}$$

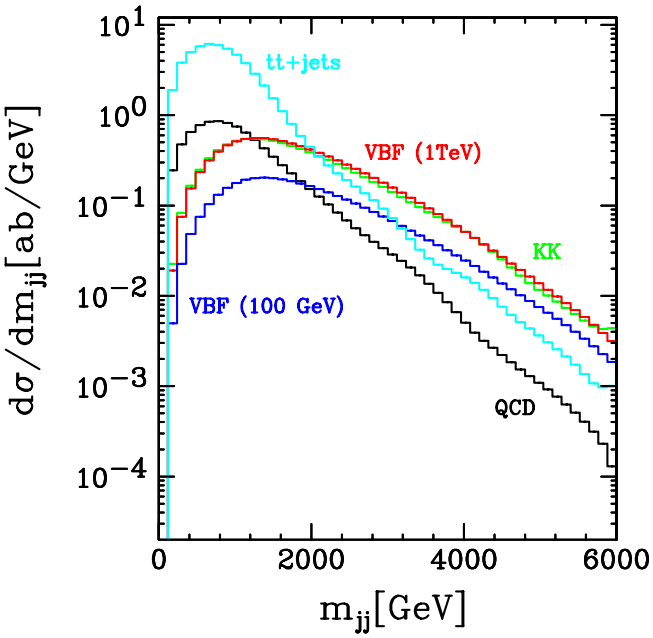

FIG. 3 (color online). Invariant mass distribution of the two tagging jets for $pp \to W^+W^-jj$ after imposing the cuts of Eqs. (10)–(17), a b veto, a CJV, and requiring $p_T(\ell) > 100$ GeV. Plotted are results for the heavy Higgs boson scenario, the Higgsless Kaluza-Klein model, and the relevant SM backgrounds.

Furthermore, the tagging jets are required to have a large invariant mass,

$$m_{jj} > m_{jj}^{\min}, \tag{18}$$

where $m_{jj}^{\min} = 1000$ GeV for the W^+W^-jj signal and background processes and $m_{jj}^{\min} = 500$ GeV for all other channels.

To illustrate the significance of the m_{jj} cut, the invariant mass distribution of the two tagging jets in $pp \to W^+W^-jj$ is shown in Fig. 3, after applying the cuts of Eqs. (10)–(17) and requiring $p_T(\ell) > 100$ GeV. For reducing the $t\bar{t}$ + jets backgrounds, additionally a b veto and a central jet veto have been imposed, as discussed below. While large invariant masses of the tagging jets are characteristic for VBF processes, QCD-induced reactions tend to peak at small values of m_{jj}. Requiring $m_{jj} > 1000$ GeV thus efficiently suppresses contributions from $t\bar{t}$ + jets and QCD $VVjj$ production with respect to the signal processes.

(III) Leptonic cuts: In all channels, the signal processes feature energetic leptons of high p_T and large invariant mass. The decay products of the backgrounds are less back-to-back in the transverse plane and are characterized by lower transverse momenta. These features suggest the application of extra selection cuts specific to each decay channel:

(i) $ZZjj \to 4\ell jj$:

$$m_{ZZ} > 500 \text{ GeV}, \qquad p_T(\ell\ell) > 0.2 \times m_{ZZ}. \tag{19}$$

Here, m_{ZZ} is the invariant mass of the four-lepton system, and $p_T(\ell\ell)$ the transverse momentum of two same-flavor charged leptons.

(ii) $ZZjj \to 2\ell 2\nu jj$:

$$m_T(ZZ) > 500 \text{ GeV}, \qquad p_T^{\text{miss}} > 200 \text{ GeV}, \tag{20}$$

with p_T^{miss} being the transverse momentum of the neutrino system and

$$m_T^2(ZZ) = [\sqrt{m_Z^2 + p_T^2(\ell\ell)} + \sqrt{m_Z^2 + (p_T^{\text{miss}})^2}]^2 - [\vec{p}_T(\ell\ell) + \vec{p}_T^{\text{miss}}]^2. \tag{21}$$

(iii) $W^{\pm}Zjj$:

$$m_T(WZ) > 500 \text{ GeV}, \qquad p_T^{\text{miss}} > 30 \text{ GeV}, \tag{22}$$

where

$$m_T^2(WZ) = [\sqrt{m^2(\ell\ell\ell) + p_T^2(\ell\ell\ell)} + |p_T^{\text{miss}}|]^2 - [\vec{p}_T(\ell\ell\ell) + \vec{p}_T^{\text{miss}}]^2, \tag{23}$$

with $m(\ell\ell\ell)$ and $p_T(\ell\ell\ell)$ denoting the invariant mass and transverse momentum of the charged-lepton system, respectively.

(iv) W^+W^-jj:

$$\begin{aligned} &p_{T\ell} > 100 \text{ GeV}, \\ &\Delta p_T(\ell\ell) = |\vec{p}_{T,\ell_1} - \vec{p}_{T,\ell_2}| > 250 \text{ GeV}, \\ &m_{\ell\ell} > 200 \text{ GeV}, \\ &\min(m_{\ell j}) > 180 \text{ GeV}, \end{aligned} \tag{24}$$

where $\Delta p_T(\ell\ell)$ is the difference between the transverse momenta of the two charged decay leptons, and $\min(m_{\ell j})$ the minimum invariant mass of a tagging jet and any charged lepton.

To motivate this set of selection cuts, we show representative distributions for the $pp \to W^+W^-jj$ channel in the following. In Fig. 4, the transverse momentum distribution of the softest charged lepton is shown after imposing the cuts of Eqs. (10)–(18), a b veto, and a central jet veto. While the heavy Higgs and the Kaluza-Klein distributions can barely be distinguished from the QCD and EW backgrounds at low transverse momenta, the signal cross sections start to deviate from the EW $WWjj$ background at about $p_{T\ell} \approx 100$ GeV. Removing events with $p_{T\ell} < 100$ GeV therefore helps to suppress irreducible back-

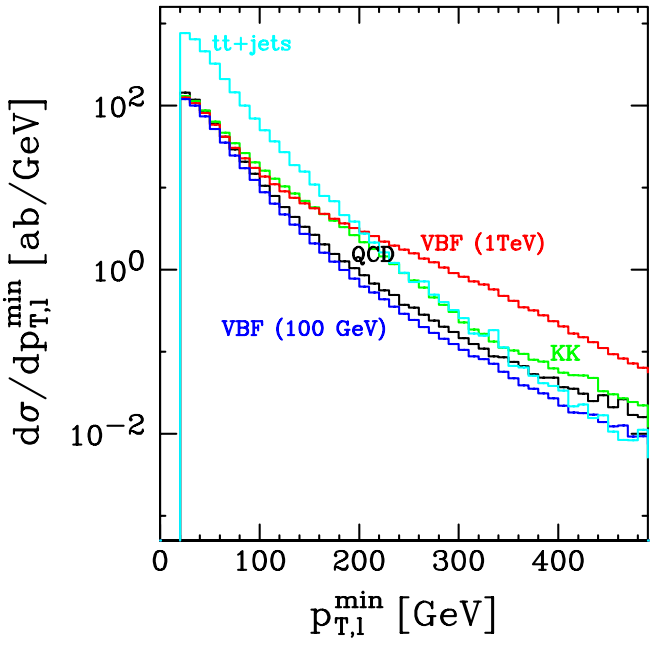

FIG. 4 (color online). Transverse momentum distribution of the softest charged lepton for $pp \to W^+W^- jj$ after imposing the cuts of Eqs. (10)–(18), a b veto, and a CJV. Plotted are results for the heavy Higgs boson scenario, the Higgsless Kaluza-Klein model, and the relevant SM backgrounds.

grounds from SM-like $W^+W^- jj$ production processes. For reducing the still sizable $t\bar{t}$ + jets cross sections, additional cuts are necessary.

Figure 5(a) displays the invariant mass distribution of the two charged final-state leptons after all inclusive and VBF cuts have been applied, and a b veto, a central jet veto, $p_T(\ell) > 100$ GeV, and $\min(m_{lj}) > 180$ GeV have been imposed. In the heavy Higgs and Kaluza-Klein signal processes, the invariant mass distribution peaks at rather large values of $m_{\ell\ell}$, while smaller invariant masses are preferred by the background processes, which therefore can be reduced considerably by requiring $m_{\ell\ell} > 200$ GeV.

Choosing the cut on the difference in the transverse momenta of the decay leptons is a subtle issue, as the peaks of the signal and background distributions are located rather closely in $\Delta p_T(\ell\ell)$; see Fig. 5(b). Selecting events with $\Delta p_T(\ell\ell) > 250$ GeV turns out to be a reasonable choice, however, which suppresses contributions from the $t\bar{t}$ + jets and the QCD $VVjj$ processes, while the Kaluza-Klein and heavy Higgs cross sections are retained to a large extent.

The cut on the minimum invariant mass of the tagging jet and any charged lepton, depicted in Fig. 6, is particularly effective in reducing the $t\bar{t}$ and $t\bar{t}j$ backgrounds, i.e. the cases where at least one of the tagging jets arises from a b quark which is a top decay product. For top quarks which are almost on mass shell, this b quark must have an invariant mass with the charged lepton from the same top-quark decay of $m_{\ell j} < m_t$. The $\min(m_{\ell j})$ cut will thus reduce the $t\bar{t}$ + jets background to mostly its $t\bar{t}jj$ component. At the same time, the signal processes are only

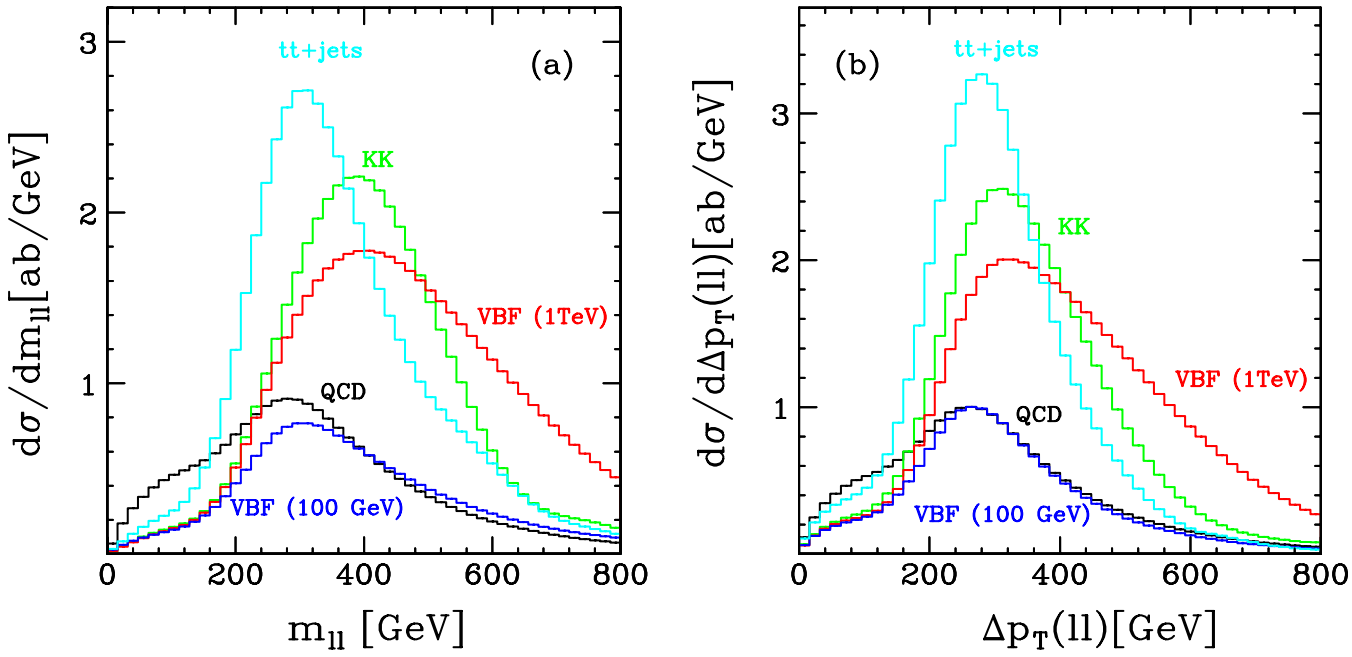

FIG. 5 (color online). Invariant mass distribution of the two charged leptons (a) and the difference between their transverse momenta (b) for the $pp \to W^+W^- jj$ process after imposing the cuts of Eqs. (10)–(18), a b veto, a CJV, and requiring $p_T(\ell) > 100$ GeV and $\min(m_{lj}) > 180$ GeV. Plotted are results for the heavy Higgs boson scenario, the Higgsless Kaluza-Klein model, and the relevant SM backgrounds.

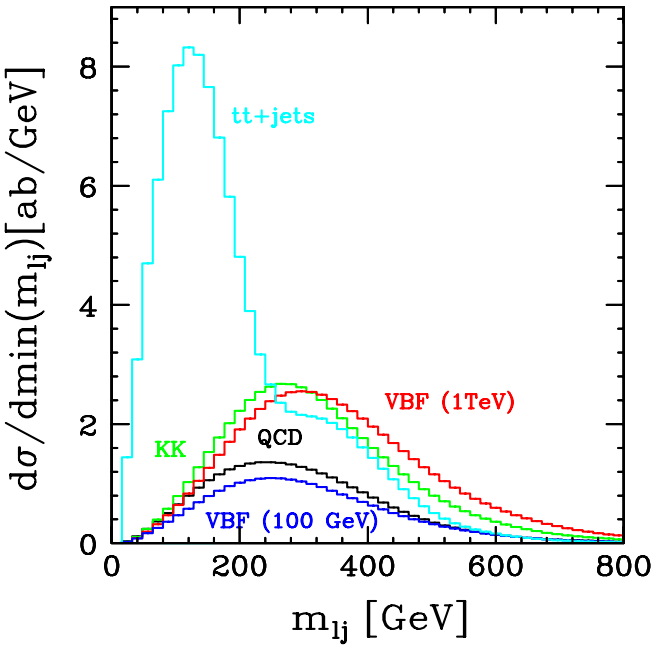

FIG. 6 (color online). Minimum invariant mass distribution of a tagging jet and a charged lepton for the $pp \to W^+W^-jj$ process after imposing the cuts of Eqs. (10)–(18), a b veto, a CJV, and requiring $p_T(\ell) > 100$ GeV. Plotted are results for the heavy Higgs boson scenario, the Higgsless Kaluza-Klein model, and the relevant SM backgrounds.

slightly affected, as their $m_{\ell j}$ shapes are peaking well above 200 GeV.

The powerful sets of selection cuts introduced so far exploit the characteristic features of VBF processes and the fact that we are looking for the decay products of massive objects or, more precisely, for low partial waves in high energy vector boson scattering. We did not impose further leptonic cuts for the $ZZjj$ and $W^\pm Zjj$ channels, because the amount of improvement in the significance of the signal would be marginal. However, in the case of $pp \to W^+W^-jj$ additional measures are necessary to suppress the overwhelming $t\bar{t}$ + jets backgrounds.

(IV) Central jet veto: QCD-induced processes tend to exhibit more jet activity in the central-rapidity region than VBF reactions with colorless weak boson exchange in the t channel. A central jet veto (CJV) can therefore be applied to reduce QCD backgrounds by eliminating events where in addition to the tagging jets at high rapidity secondary jets with a high transverse momentum are found in the central regions of the detector. We veto any such activity by discarding all events with an extra veto jet of

$$p_{Tj}^{\text{veto}} > 25 \text{ GeV}, \tag{25}$$

located in the gap region between the two tagging jets,

TABLE II. Assumed b-tagging efficiencies as functions of the transverse momentum of the jet for different rapidity ranges.

p_{Tj}^{veto} (GeV)	$1.4 < \lvert\eta_j^{\text{veto}}\rvert < 2.4$	$\lvert\eta_j^{\text{veto}}\rvert < 1.4$
30–50	60%	70%
50–80	65%	75%
80–120	70%	80%
120–170	70%	80%
>170	65%	75%

$$\eta_{j,\min}^{\text{tag}} < \eta_j^{\text{veto}} < \eta_{j,\max}^{\text{tag}}. \tag{26}$$

In our simulations we do not yet model extra QCD radiation which might be subject to the central jet veto. Such refinements are beyond the scope of the present work. However, the $t\bar{t}j$ and $t\bar{t}jj$ background processes typically have additional b-quark jets from top-quark decay in the central region. The CJV thus is very effective in reducing these backgrounds.

(V) b-tagging jet veto: Discrimination between jets originating from b quarks and those emerging from light quarks or gluons by efficient b tagging helps additionally to suppress $t\bar{t}$ + jets backgrounds in the W^+W^-jj channel: we eliminate any events where at least one of the tagging jets is identified as arising from a b quark. We use the results of a CMS analysis [76] for our assumptions on b-veto efficiencies and mistagging probabilities. For a 10% mistagging probability per jet one finds b-veto efficiencies in the range 60%–80%, depending on the transverse momentum and pseudorapidity of the jet as listed in Table II.

IV. RESULTS AND DISCUSSION

We now turn to a discussion of numerical results for the signal and background processes of the scenarios discussed in the previous sections. In all cases the cross sections correspond to two generations of charged leptons and three neutrino species for $Z \to \bar{\nu}\nu$. They are listed in Tables III, IV, V, VI, and VII for all processes contributing to a specific leptonic final state, after different sets of selection cuts have been applied. The impact on inclusive cross sections of only the VBF cuts or only the leptonic cuts is shown in the lines labeled "INC. + VBF" and "INC. + LEP.," respectively. In each case, we consider the QCD $VVjj$ background, EW $VVjj$ production assuming a light or a heavy Higgs boson, and a warped Higgsless scenario with additional spin-one resonances. For the W^+W^-jj channel also the $t\bar{t}$ + jets background is given and the impact of CJV and b-veto cuts on the cross section after inclusive and VBF cuts is also shown. In Table VIII, results for $t\bar{t}$, $t\bar{t}j$, and $t\bar{t}jj$ production are listed separately to better illustrate the impact of the individual contributions.

In all channels, VBF cuts reduce the QCD $VVjj$ backgrounds efficiently, decreasing inclusive production rates by factors of 25–85 as shown in the respective second lines of Tables III, IV, V, VI, and VII. VBF cuts are even more efficient in the case of the $t\bar{t}$, $t\bar{t}j$, and $t\bar{t}jj$ background processes, as illustrated by Table VIII. At the same time, rates for the heavy and light Higgs boson scenarios as well as for the Higgsless Kaluza-Klein model have decreased by a factor of 2–3 only.

Imposing leptonic cuts, on the other hand, helps to suppress EW backgrounds, while the respective signal processes remain substantial, as apparent from the third rows of Tables III, IV, V, VI, and VII. Combining the leptonic and VBF cuts one finds sufficient background suppression for the $ZZjj$ and $WZjj$ final states, as shown in the fourth rows of Tables III, IV, V, and VI. For the $t\bar{t}$ + jets backgrounds to W^+W^-jj final states the impact of the leptonic cuts is even more pronounced than the effect of the VBF cuts. However, total rates are still much higher for the

TABLE III. Cross sections (in fb) for various $ZZjj \to 4\ell jj$ production processes with different Higgs boson masses and the Higgsless Kaluza-Klein scenario, after different levels of selection cuts have been applied, as defined in Sec. III. Statistical errors in all cases are well below 0.5%.

Level of cuts	QCD	VBF $m_H = 100$ GeV	VBF $m_H = 1$ TeV	KK
INCLUSIVE	3.83	0.232 3	0.310 1	0.272 5
INC. + VBF	0.075 2	0.088 3	0.150 3	0.111 52
INC. + LEP.	0.375 5	0.028 27	0.083 02	0.042 27
INC. + VBF + LEP.	0.009 51	0.011 71	0.059 48	0.021 47

TABLE IV. Cross sections (in fb) for various $ZZjj \to 2\ell 2\nu jj$ production processes with different Higgs boson masses and the Higgsless Kaluza-Klein scenario, after different levels of selection cuts have been applied. Statistical errors in all cases are well below 0.5%.

Level of cuts	QCD	VBF $m_H = 100$ GeV	VBF $m_H = 1$ TeV	KK
INCLUSIVE	36.13	1.961	2.482	2.260
INC. + VBF	0.867	0.778 8	1.196	0.953 1
INC. + LEP.	1.717	0.116 3	0.4230	0.185 2
INC. + VBF + LEP.	0.0518	0.049 07	0.3194	0.098 83

TABLE V. Cross sections (in fb) for various W^+Zjj production processes with different Higgs boson masses and the Higgsless Kaluza-Klein scenario, after different levels of selection cuts have been applied. Statistical errors in all cases are well below 0.5%.

Level of cuts	QCD	VBF $m_H = 100$ GeV	VBF $m_H = 1$ TeV	KK
INCLUSIVE	54.96	1.834	1.897	2.718
INC. + VBF	2.189	0.6933	0.7382	1.273
INC. + LEP.	4.301	0.2382	0.2599	0.9161
INC. + VBF + LEP.	0.1719	0.0888	0.1077	0.5435

TABLE VI. Cross sections (in fb) for various W^-Zjj production processes with different Higgs boson masses and the Higgsless Kaluza-Klein scenario, after different levels of selection cuts have been applied. Statistical errors in all cases are well below 0.5%.

Level of cuts	QCD	VBF $m_H = 100$ GeV	VBF $m_H = 1$ TeV	KK
INCLUSIVE	37.48	1.107 2	1.144 5	1.5863
INC. + VBF	1.304	0.379 8	0.404 8	0.6784
INC. + LEP.	2.385	0.123 3	0.134 4	0.4828
INC. + VBF + LEP.	0.0838	0.043 24	0.052 72	0.2758

TABLE VII. Cross sections (in fb) for various W^+W^-jj production processes with different Higgs boson masses and the Higgsless Kaluza-Klein scenario after different levels of selection cuts have been applied. Also given is the sum of the $t\bar{t}$, $t\bar{t}j$, and $t\bar{t}jj$ backgrounds for $m_t = 172.5$ GeV and $m_H = 100$ GeV. Statistical errors are well below 0.5% for the W^+W^-jj processes and below 1% for $t\bar{t}$ + jets.

Level of cuts	$t\bar{t}$ + jets	QCD	VBF $m_H = 100$ GeV	VBF $m_H = 1$ TeV	KK
INCLUSIVE	28 710.0	504.5	16.76	18.55	19.80
INC. + VBF	228.667	5.918	5.063	6.165	6.536
INC. + LEP.	27.4090	6.72	0.828	1.620	1.702
INC. + VBF + b VETO	64.055	5.473	4.77	5.86	6.22
INC. + VBF + CJV	43.197	⋯	⋯	⋯	⋯
⋯ + b VETO	24.025	5.47	4.772	5.856	6.217
⋯ + LEP.	0.381 644	0.202	0.1969	0.7011	0.588

backgrounds than for the corresponding signal process. Thus, additional cuts have to be applied for the W^+W^-jj production mode. In order to reduce the large $t\bar{t}$ + jets backgrounds we make use of a b veto and a CJV. We discard all events where one or both tagging jets can be identified as b jets, allowing for an overall mistagging probability of 10% for light partons with $p_T > 30$ GeV and $|\eta| < 2.4$. This results in a reduction of less than 10% for the signal and all backgrounds apart from $t\bar{t}$ + jets. The b veto reduces these top-induced backgrounds by a factor of 2–4. The CJV is particularly efficient for the $t\bar{t}jj$ process. In this case, an additional reduction factor of 18 is obtained. The last row of Table VIII shows that after the application of all cuts the $t\bar{t}$ + jets background rates are comparable in size to those of the other individual backgrounds.

In Tables IX and X, the signal and combined background cross sections σ_S and σ_B are listed together with the ratios S/B, $S/\sqrt{B}$, and $S/\sqrt{S+B}$, where S and B denote signal and background rates, respectively. They are calculated for a luminosity of 300 fb^{-1} from the cross sections tabulated in Tables III, IV, V, VI, VII, and VIII, after all selection cuts have been applied, with the signal defined according to Eqs. (5) and (6). The W^-Zjj channel exhibits features very similar to the related W^+Zjj mode, while its production rates are always smaller by approximately a factor of 2, which is due to the size of the parton distribution functions of the dominant subprocesses for the respective production modes. In Tables IX and X we therefore combine the W^+Zjj and the W^-Zjj channels to enhance the statistical significance of the $W^\pm Zjj$ mode.

TABLE VIII. Cross sections (in fb) for the $t\bar{t} + nj$ production processes, where $n = 0$, 1, 2, with $m_t = 172.5$ GeV and $m_H = 100$ GeV, after different levels of selection cuts have been applied. Statistical errors in all cases are well below 1%.

Level of cuts	$t\bar{t}$	$t\bar{t}j$	$t\bar{t}jj$	Sum ($t\bar{t}$ + jets)
INCLUSIVE	13 850.0	13 260.0	1600.0	28 710.0
INC. + VBF	1.967	131.4	95.3	228.667
INC. + LEP.	0.0490	3.02	24.34	27.4090
INC. + VBF + b VETO	0.915	38.57	24.57	64.055
INC. + VBF + CJV	1.967	35.82	5.41	43.197
⋯ + b VETO	0.915	18.24	4.87	24.025
⋯ + LEP.	0.000 844	0.0518	0.329	0.381 644

TABLE IX. Cross sections for the heavy Higgs boson signal and overall background for various channels (in fb) after all selection cuts have been applied. Also listed are several ratios for signal and background rates together with the number of signal and background events for an assumed integrated luminosity of 300 fb^{-1} at the LHC.

Process	σ_S	σ_B	S/B	$S/\sqrt{B}$	$S/\sqrt{S+B}$	$N^{\rm SM}_{\rm signal}$	$N_{\rm bkgd.}$
$ZZjj \to 4\ell jj$	0.048	0.021	2.2	5.7	3.1	14	6
$ZZjj \to 2l2\nu jj$	0.27	0.10	2.7	14.8	7.7	81	30
W^+W^-jj	0.51	0.78	0.6	10.0	7.8	153	234
$W^\pm Zjj$	0.031	0.386	0.1	0.9	0.8	9	116

TABLE X. Cross sections for the Higgsless Kaluza-Klein scenario and overall background for various channels (in fb), after all selection cuts have been applied. Also listed are several ratios for signal and background rates together with the number of signal and background events for an assumed integrated luminosity of 300 fb^{-1} at the LHC.

Process	σ_S	σ_B	S/B	$S/\sqrt{B}$	$S/\sqrt{S+B}$	$N_{\text{signal}}^{\text{SM}}$	$N_{\text{bkgd.}}$
$W^{\pm}Zjj$	0.68	0.39	1.7	18.9	11.4	204	117
W^+W^-jj	0.40	0.78	0.5	7.9	6.4	120	234
$ZZjj \to 4\ell jj$	0.009	0.021	0.4	1.1	0.9	3	6
$ZZjj \to 2\ell 2\nu jj$	0.05	0.10	0.5	2.7	2.2	15	30

Considering the SM with a heavy Higgs boson as a prototype for scenarios with a broad scalar, isoscalar resonance, an indicator for the LHC sensitivity is provided by the cross section enhancement in the $ZZjj$ and W^+W^-jj channels for VBF with $m_H = 1$ TeV. These two channels provide excellent possibilities for the study of strongly interacting gauge boson systems via scalar resonances; see Table IX. Particularly encouraging is the signal rate for the $ZZjj \to 2\ell 2\nu jj$ mode. The absence of a significant enhancement in the $WZjj$ channel is a crucial factor in identifying the isoscalar character of such a resonance.

A 5σ statistical significance, defined here as $S/\sqrt{B} = 5\sigma$, for a signal with a heavy Higgs boson can already be obtained with an integrated luminosity of 240, 35, and 75 fb^{-1}, respectively, for the $ZZjj \to 4\ell jj$, the $ZZjj \to 2\ell 2\nu jj$, and the W^+W^-jj processes. It should be noted, however, that event rates for $ZZ \to 4$ charged leptons are very small, and Poisson significances would be substantially smaller. $W^{\pm}Zjj$ production, with heavy Higgs boson contributions entering via t- and u-channel exchange diagrams only, is hardly affected by the Higgs resonance. No significant deviation from background is expected in this channel for the heavy Higgs scenario.

In contrast, the warped Higgsless Kaluza-Klein model with a tower of additional vector resonances can be studied most easily via the $W^{\pm}Zjj$ and W^+W^-jj modes, as shown in Table X. In the $W^{\pm}Zjj$ channel, the first of the W_k resonances, W_2, can be observed. Two Z_k resonances, which are difficult to disentangle, Z_2 and Z_3, are accessible in the W^+W^-jj process. A 5σ statistical significance for the Higgsless signal, calculated using the same formula as in the heavy Higgs boson case, can be obtained with a minimal integrated luminosity of 25 and 125 fb^{-1}, respectively, for the $W^{\pm}Zjj$ and the W^+W^-jj processes for our choice of the model parameter $R = 9.75 \times 10^{-9}$. The two $ZZjj$ channels are much less sensitive to this model, since in these production modes the W_k Kaluza-Klein excitations occur only in t- and u-channel exchange diagrams. A similar study for the W^+W^-jj channel in the context of a Higgsless Kaluza-Klein scenario has been performed in Ref. [77], yielding a signal significance of comparable size.

Altogether, a reasonable number of signal events can be achieved at the LHC for an integrated luminosity of 300 fb^{-1}; see Tables IX and X. Our cuts have considerably reduced backgrounds, so that even a relatively small number of excess signal events should be observable. The $W^{\pm}Zjj$ channel *per se* is not sensitive to a scalar resonance like a 1 TeV Higgs boson. Similarly, the $ZZjj$ mode is barely sensitive to the $W^{\pm}$ KK mode. It is however the combined analysis of all channels that eventually allows one to select between the models as distinct realizations of electroweak symmetry breaking.

In addition to the signal and background rates listed above, we have studied various kinematic distributions for each production process. Representative results are presented in the following, with histograms corresponding to the cross sections listed in Tables III, IV, V, VI, and VII. Because of the large $t\bar{t}$ + jets cross sections, the W^+W^-jj mode constitutes the biggest challenge. In Fig. 5(a), we have shown the invariant mass distribution of the two charged leptons in $pp \to W^+W^-jj$ after the application of general selection cuts. At this level of cuts, the $t\bar{t}$ + jets background was still sizable. If additionally all process-specific cuts of Eq. (24) are imposed, the $t\bar{t}$ + jets cross sections can be further reduced, while the signal distributions are barely affected; cf. Figure 7(a).

In Fig. 7(b), the cluster transverse mass of the produced W^+W^- system, defined by

$$m_T^2(WW) = [\sqrt{m^2(\ell\ell) + p_T^2(\ell\ell)} + |p_T^{\text{miss}}|]^2 - [\vec{p}_T(\ell\ell) + \vec{p}_T^{\text{miss}}]^2, \quad (27)$$

is shown. Similar to the $m_{\ell\ell}$ distribution, QCD and EW $VVjj$ backgrounds are small, and $t\bar{t}$ + jets is well under control. The Kaluza-Klein scenario we consider exhibits a pronounced resonance peak, well above the backgrounds. The heavy Higgs cross section is distributed more broadly in $m_T(WW)$, but still well distinguishable.

The heavy Higgs scenario can also be well identified in the $ZZjj$ production modes, which are, however, less sensitive to Kaluza-Klein resonances as discussed above. Figure 8(a) shows the invariant mass distribution of the four charged leptons in $pp \to ZZjj \to 4\ell jj$ after all process-specific selection cuts have been applied. The impact of the heavy Higgs resonance is evident at $m_{ZZ} = 1000$ GeV, where all backgrounds are small. The Kaluza-Klein cross section exceeds the QCD and continuum EW

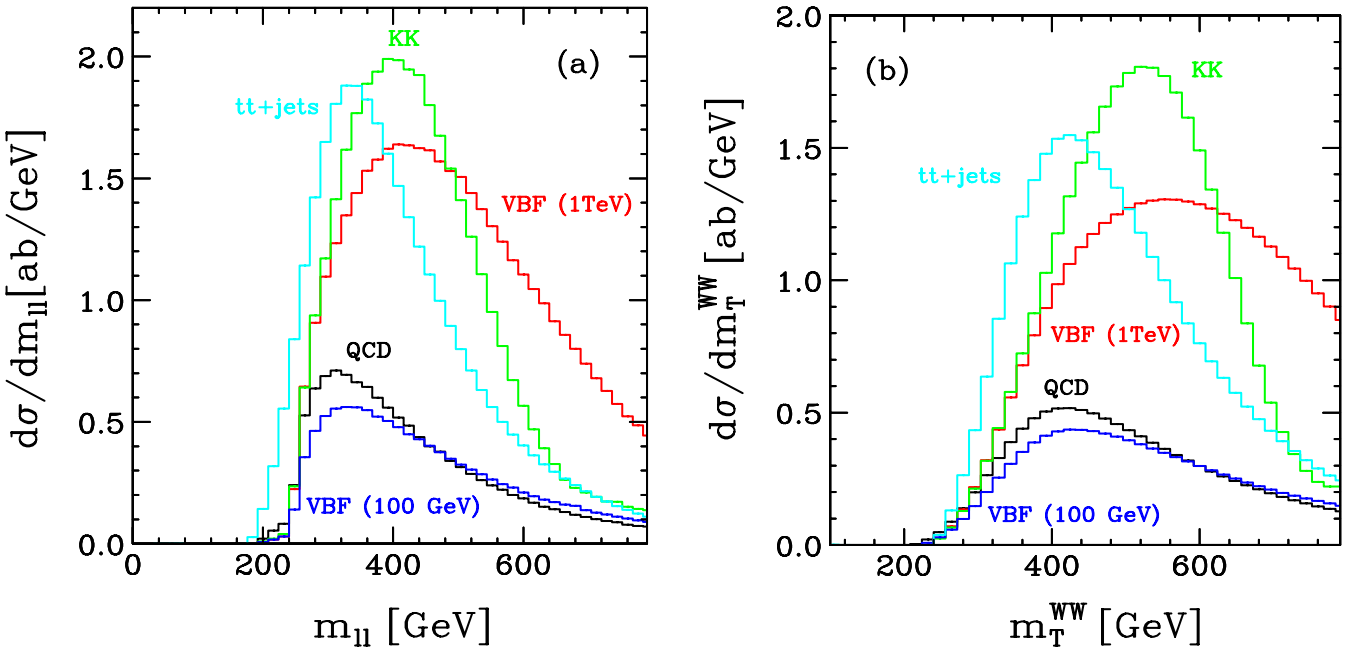

FIG. 7 (color online). Invariant mass distribution of the two charged leptons (a) and cluster transverse mass distribution of the W^+W^- system (b) for the $pp \to W^+W^- jj$ process after imposing all levels of cuts.

results, but does not exhibit a characteristic resonance behavior. The Higgsless model's excess over the EW continuum can be understood from the absence of an isoscalar exchange contribution to weak gauge boson scattering, which in the SM enters with an amplitude of opposite phase as the gauge boson exchange graphs. Another distinction can be observed in the invariant mass distribution of the tagging jets displayed in Fig. 8(b). The excess events from enhanced VBF production correlate with large dijet invariant masses, while the QCD background mostly resides at $m_{jj} < 1$ TeV and rapidly falls off as m_{jj} increases.

This behavior is completely independent of the gauge boson decay, as illustrated by Fig. 9(a), where the m_{jj} distribution is shown for the $ZZjj \to 2\ell 2\nu jj$ mode.

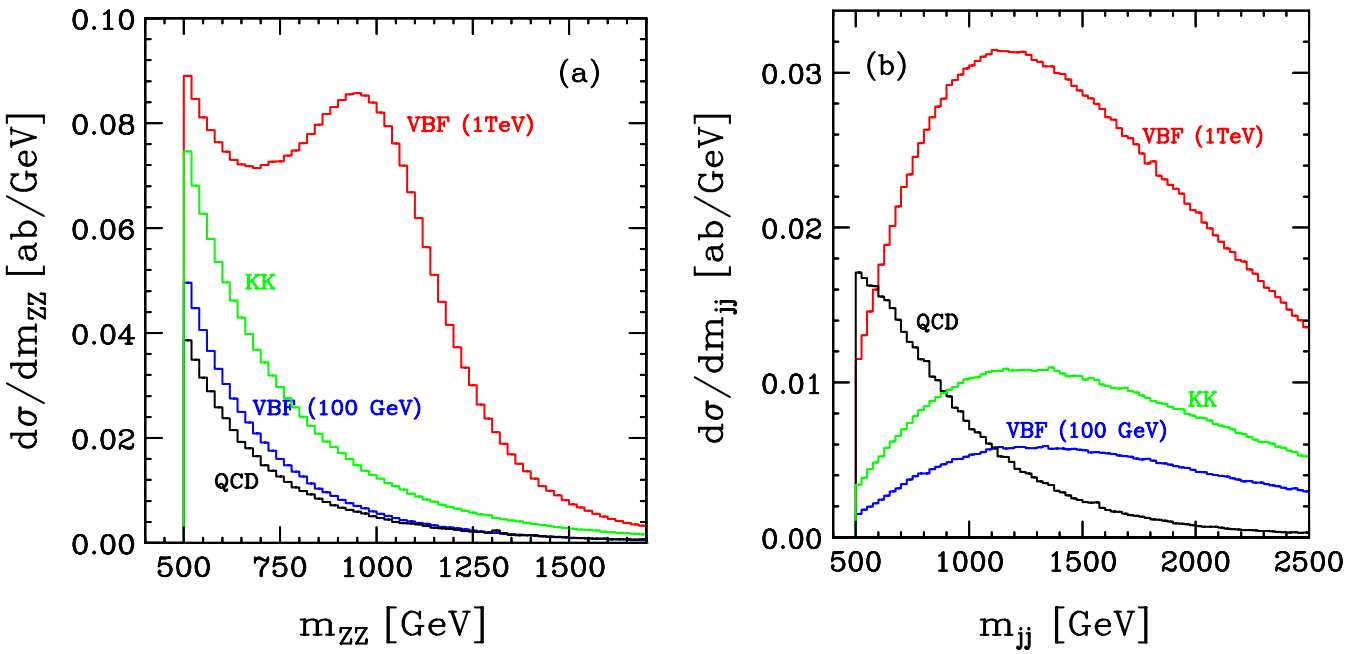

FIG. 8 (color online). Invariant mass distribution of the four charged leptons (a) and of the two tagging jets (b) for the $pp \to ZZjj \to 4\ell jj$ process after imposing all levels of cuts.

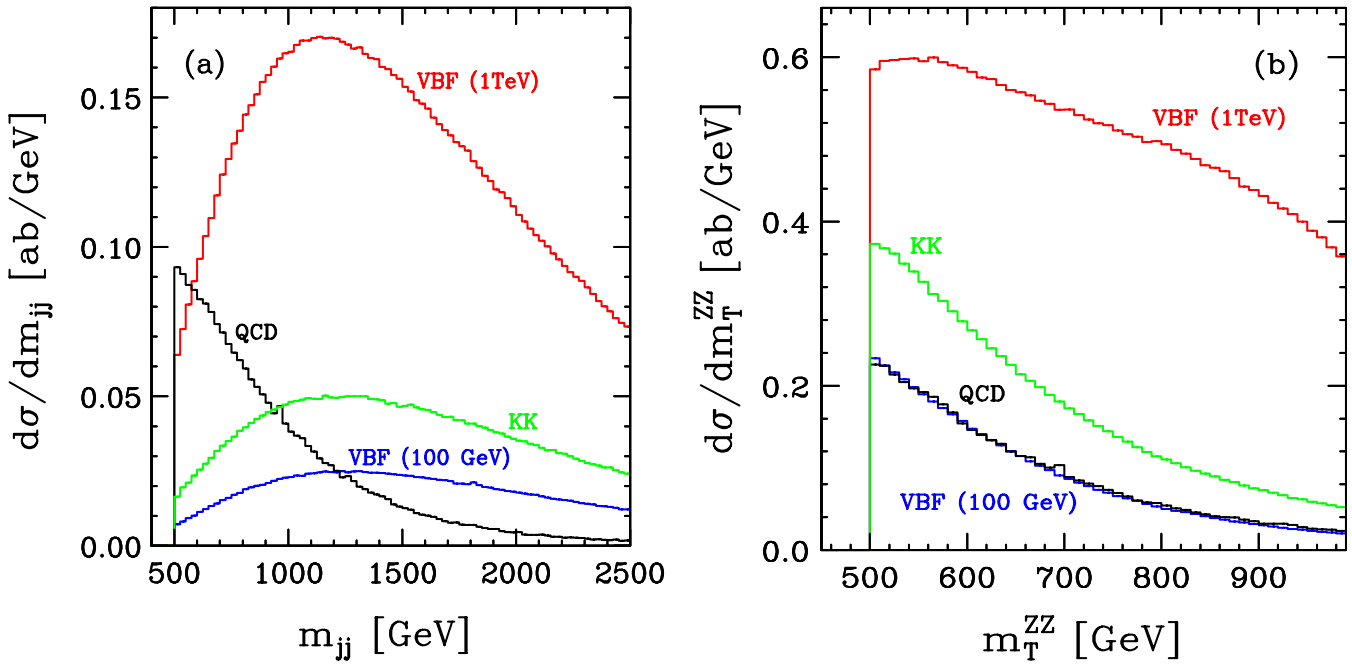

FIG. 9 (color online). Invariant mass distribution of the two tagging jets (a) and cluster transverse mass distribution of the ZZ system (b) for the $pp \to ZZjj \to 2\ell 2\nu jj$ process after imposing all levels of cuts.

Apparently, the shapes of the invariant mass distribution are identical to the $ZZjj \to 4\ell jj$ case. The overall normalization differs due to the $Z \to \nu\bar{\nu}$ branching ratio exceeding the one for $Z \to \ell^+\ell^-$. Figure 9(b) illustrates the cluster transverse mass of the ZZ system in the $2\ell 2\nu jj$ decay mode. Similar to the m_{ZZ} distribution in $pp \to ZZjj \to 4\ell jj$, the heavy Higgs cross section dominates over all backgrounds. However, the Higgs resonance does not manifest itself in a pronounced peak, but is smeared out over a large range in $m_T(ZZ)$.

The most distinctive signatures of isovector Kaluza-Klein excitations are observed in the $W^{\pm}Zjj$ mode, since these heavy spin-one states contribute to resonant $W^{\pm}Z$ scattering, which does not occur in scenarios with a scalar

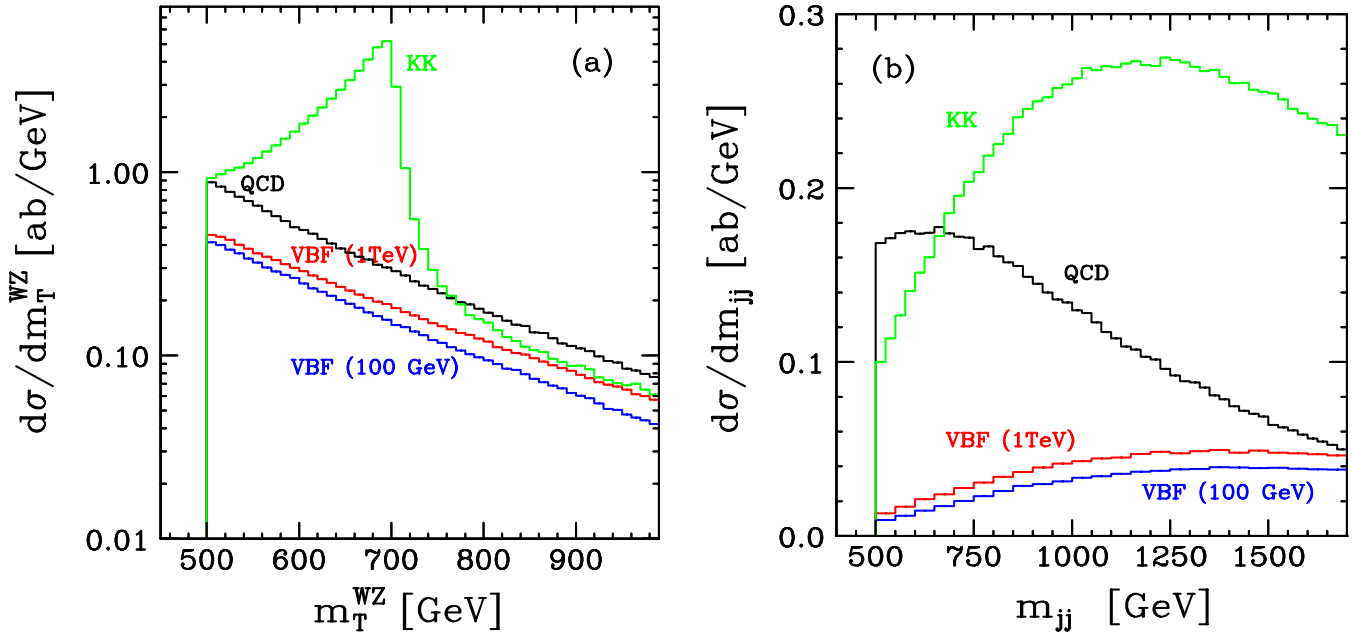

FIG. 10 (color online). Cluster transverse mass distribution of the W^+Z system (a) and invariant mass distribution of the two tagging jets (b) for the $pp \to W^+Zjj$ process after imposing all levels of cuts.

Higgs boson. This is illustrated by Fig. 10(a), which shows the cluster transverse mass distribution for the W^+Zjj case. The $m_T(WZ)$ distribution exhibits a characteristic peak at about 700 GeV due to the impact of the first massive Kaluza-Klein excitation W_2. The QCD and EW backgrounds as well as the heavy Higgs cross section are smoothly distributed over $m_T(WZ)$. As expected, the VBF cross sections for the $m_H = 100$ GeV and the $m_H = 1$ TeV case are very similar, because the scalar Higgs boson contributes to W^+Z scattering only via nonresonant diagrams. Also for W^+Zjj production, the invariant mass distribution of the two tagging jets, as shown in Fig. 10(b), shows the characteristic distinction between QCD backgrounds and VBF processes. Shapes for W^-Zjj production are almost identical to the W^+Zjj case and therefore not displayed here.

In summary, signatures of a heavy Higgs boson scenario as well as of Kaluza-Klein excitations should be observable in gauge boson scattering processes at the LHC. While an isoscalar resonance like a heavy Higgs boson manifests itself most distinctively in the W^+W^-jj and the $ZZjj$ channels, a Higgsless scenario with isovector resonances, such as the Kaluza-Klein model which we have considered, can be studied best in the $W^\pm Zjj$ channel. A multivariate analysis with full detector simulation might yield a slightly different shape of the distributions and total rates. However, our conclusions on the observability of strong interaction signatures should remain valid.

V. CONCLUSIONS

The origin of electroweak symmetry breaking is still unknown. While a perturbative Higgs sector with a light SM-like Higgs boson is a preferred solution at present, experimental tests are needed to probe other scenarios where new strong interactions are responsible for the weak gauge boson masses. With the luminosity and energy available at the LHC the search for such scenarios becomes feasible via studies of weak boson scattering as realized in vector boson fusion processes.

We have performed a broad study of the possibility to probe the strongly interacting electroweak symmetry breaking sector in gauge boson scattering reactions leading to $ZZjj$, $W^\pm Zjj$, and W^+W^-jj final states at the LHC, using only leptonic decay modes. By performing full tree-level simulations of the dominant backgrounds, at a level where double forward jet-tagging acceptances can be reliably calculated, we have established selection cuts which allow one to isolate the strong weak boson scattering signals. We have found that, for each of the models we considered, an observable excess of events occurs in at least one of the production modes, after three years of running with an annual luminosity of 100 fb^{-1}. As compared to Ref. [19], higher signal rates for a SM-like 1 TeV Higgs boson could be obtained with loosened leptonic cuts by tagging two jets of high transverse momenta. Defining such high acceptance signal regions for the various vector boson fusion channels and providing realistic background estimates in these regions was a second goal of our work. These results can now be used for further studies, be it of other scenarios for weak boson scattering, for the assessment of higher order QCD corrections, or for refinements such as improved central jet veto techniques. We should stress that our analysis has been conservative, as a central jet veto offers promising prospects for a further enhancement of the signal-to-background ratio. From related studies on $pp \to Z + 2$jets and $pp \to H + 2$jets [78,79] one expects additional suppression of the QCD backgrounds by about 70%, while around 90% of the VBF signal are retained when a central jet veto is imposed.

In the search regions defined in Sec. III, ignoring improvements from a central jet veto on the QCD backgrounds, even the SM light Higgs scenario yields weak boson fusion signal cross sections which are of the same order as the QCD backgrounds, with signal-to-background ratios of 1:1 for $ZZjj$ final states, 1:2 for the higher statistics $WZjj$ mode, and 1:3 for W^+W^-jj. With expected statistical samples of 36, 116, and 234 signal plus background events, respectively, in 300 fb^{-1} of data, an increase of the VBF cross section by a factor of 2 in any of these channels should be observable at the LHC. Our conclusions are thus valid beyond the details of the models considered and will certainly apply to any scalar or vector resonances of sufficient size but general peak location.

Should a light Higgs boson be found rather than first signatures of strong gauge boson interactions, the precise measurement of event rates at high invariant mass is essential to ensure that the Higgs boson indeed cures the bad high energy behavior of gauge boson scattering processes as predicted by the SM. Given the results mentioned above, a measurement of the high vector boson pair invariant mass cross section in several vector boson fusion channels, with a statistical accuracy of order 30%, seems possible after several years of LHC running. Improvements on this result appear feasible, in particular, with a more realistic calculation of central jet veto acceptances for QCD-induced background events, which make use of the elevated level of central soft gluon radiation in such events. We leave such refinements to future work.

ACKNOWLEDGMENTS

We are grateful to N. Kauer for making his computer code for $t\bar{t}$ + jets available for comparison with the HELACPHEGAS package. We furthermore would like to thank G. Klämke for interesting discussions. Our work was supported by the Japan Society for the Promotion of Science (JSPS) and by the Deutsche Forschungsgemeinschaft via the Sonderforschungsbereich/Transregio SFB/TR-9 "Computational Particle Physics." M. W. was funded in part by the RTN European Programme MRTN-CT-2006-

035505 HEPTOOLS—Tools and Precision Calculations for Physics Discoveries at Colliders, B. J. by the Initiative and Networking Fund of the Helmholtz Association, Contract No. HA-101 (''Physics at the Terascale''), and C. E. by ''CETA Strukturiertes Promotionskolleg.''

[1] ATLAS Collaboration, Technical Design Report No. CERN-LHCC-99-15, Vol. 2.
[2] G. L. Bayatian *et al.* (CMS Collaboration), J. Phys. G **34**, 995 (2007).
[3] M. J. G. Veltman, Acta Phys. Pol. B **8**, 475 (1977).
[4] B. W. Lee, C. Quigg, and H. B. Thacker, Phys. Rev. Lett. **38**, 883 (1977).
[5] B. W. Lee, C. Quigg, and H. B. Thacker, Phys. Rev. D **16**, 1519 (1977).
[6] F. Englert and R. Brout, Phys. Rev. Lett. **13**, 321 (1964).
[7] P. W. Higgs, Phys. Rev. Lett. **13**, 508 (1964).
[8] G. S. Guralnik, C. R. Hagen, and T. W. B. Kibble, Phys. Rev. Lett. **13**, 585 (1964).
[9] M. S. Chanowitz and M. K. Gaillard, Phys. Lett. **142B**, 85 (1984).
[10] M. S. Chanowitz and M. K. Gaillard, Nucl. Phys. **B261**, 379 (1985).
[11] M. S. Chanowitz, Annu. Rev. Nucl. Part. Sci. **38**, 323 (1988).
[12] C. Csaki, C. Grojean, H. Murayama, L. Pilo, and J. Terning, Phys. Rev. D **69**, 055006 (2004).
[13] C. Csaki, C. Grojean, L. Pilo, and J. Terning, Phys. Rev. Lett. **92**, 101802 (2004).
[14] K. Agashe, A. Delgado, M. J. May, and R. Sundrum, J. High Energy Phys. 08 (2003) 050.
[15] L. Randall and R. Sundrum, Phys. Rev. Lett. **83**, 3370 (1999).
[16] V. D. Barger, K. Cheung, T. Han, and D. Zeppenfeld, Phys. Rev. D **44**, 2701 (1991).
[17] V. D. Barger, K. Cheung, T. Han, and D. Zeppenfeld, Phys. Rev. D **48**, 5433 (1993).
[18] J. Bagger *et al.*, Phys. Rev. D **49**, 1246 (1994).
[19] J. Bagger *et al.*, Phys. Rev. D **52**, 3878 (1995).
[20] D. L. Rainwater and D. Zeppenfeld, J. High Energy Phys. 12 (1997) 005.
[21] D. L. Rainwater, D. Zeppenfeld, and K. Hagiwara, Phys. Rev. D **59**, 014037 (1998).
[22] D. L. Rainwater and D. Zeppenfeld, Phys. Rev. D **60**, 113004 (1999).
[23] N. Kauer, T. Plehn, D. L. Rainwater, and D. Zeppenfeld, Phys. Lett. B **503**, 113 (2001).
[24] N. Kauer, Phys. Rev. D **67**, 054013 (2003).
[25] E. Accomando, A. Ballestrero, S. Bolognesi, E. Maina, and C. Mariotti, J. High Energy Phys. 03 (2006) 093.
[26] A. Alves, O. J. P. Eboli, M. C. Gonzalez-Garcia, and J. K. Mizukoshi, arXiv:0810.1952.
[27] A. Birkedal, K. Matchev, and M. Perelstein, Phys. Rev. Lett. **94**, 191803 (2005).
[28] H.-J. He *et al.*, Phys. Rev. D **78**, 031701 (2008).
[29] H. Davoudiasl, J. L. Hewett, B. Lillie, and T. G. Rizzo, Phys. Rev. D **70**, 015006 (2004).
[30] K. Agashe *et al.*, Phys. Rev. D **76**, 115015 (2007).
[31] K. Agashe, S. Gopalakrishna, T. Han, G.-Y. Huang, and A. Soni, arXiv:0810.1497.
[32] E. Farhi and L. Susskind, Phys. Rep. **74**, 277 (1981).
[33] D. B. Kaplan, H. Georgi, and S. Dimopoulos, Phys. Lett. **136B**, 187 (1984).
[34] D. B. Kaplan and H. Georgi, Phys. Lett. B **136**, 183 (1984).
[35] A. Manohar and H. Georgi, Nucl. Phys. B **234**, 189 (1984).
[36] J. Erler and P. Langacker, Acta Phys. Pol. B **39**, 2595 (2008).
[37] R. Barate *et al.*, Phys. Lett. B **565**, 61 (2003).
[38] M. E. Peskin and T. Takeuchi, Phys. Rev. Lett. **65**, 964 (1990).
[39] M. E. Peskin and T. Takeuchi, Phys. Rev. D **46**, 381 (1992).
[40] R. Barbieri, A. Pomarol, R. Rattazzi, and A. Strumia, Nucl. Phys. **B703**, 127 (2004).
[41] M. E. Peskin and J. D. Wells, Phys. Rev. D **64**, 093003 (2001).
[42] K. Arnold *et al.*, arXiv:0811.4559, http://www-itp.particle.uni-karlsruhe.de/~vbfnloweb/.
[43] C. Englert, Diploma thesis, Karlsruhe University, 2007, http://www-itp.particle.uni-karlsruhe.de/prep/diploma/PSFiles/Diplom_Englert.ps.gz.
[44] C. Englert, B. Jager, and D. Zeppenfeld, J. High Energy Phys. 03 (2009) 060.
[45] J. M. Maldacena, Adv. Theor. Math. Phys. **2**, 231 (1998).
[46] N. Arkani-Hamed, M. Porrati, and L. Randall, J. High Energy Phys. 08 (2001) 017.
[47] R. Rattazzi and A. Zaffaroni, J. High Energy Phys. 04 (2001) 021.
[48] R. S. Chivukula, H. J. He, M. Kurachi, E. H. Simmons, and M. Tanabashi, Phys. Rev. D **78**, 095003 (2008).
[49] N. Arkani-Hamed, A. G. Cohen, and H. Georgi, Phys. Lett. B **513**, 232 (2001).
[50] G. Cacciapaglia, C. Csaki, C. Grojean, and J. Terning, Phys. Rev. D **71**, 035015 (2005).
[51] R. Sekhar Chivukula, E. H. Simmons, H.-J. He, M. Kurachi, and M. Tanabashi, Phys. Rev. D **72**, 015008 (2005).
[52] A. Kanaki and C. G. Papadopoulos, Comput. Phys. Commun. **132**, 306 (2000).
[53] C. G. Papadopoulos, Comput. Phys. Commun. **137**, 247 (2001).
[54] C. G. Papadopoulos and M. Worek, Eur. Phys. J. C **50**, 843 (2007).
[55] A. Cafarella, C. G. Papadopoulos, and M. Worek, arXiv:0710.2427.
[56] http://helac-phegas.web.cern.ch/helac-phegas/.

[57] J. Alwall *et al.*, Comput. Phys. Commun. **176**, 300 (2007).
[58] T. Gleisberg, F. Krauss, C. G. Papadopoulos, A. Schälicke, and S. Schumann, Eur. Phys. J. C **34**, 173 (2004).
[59] J. Alwall *et al.*, Eur. Phys. J. C **53**, 473 (2008).
[60] F. Maltoni and T. Stelzer, J. High Energy Phys. 02 (2003) 027.
[61] J. Alwall *et al.*, J. High Energy Phys. 09 (2007) 028.
[62] J. Pumplin *et al.*, J. High Energy Phys. 07 (2002) 012.
[63] D. Stump *et al.*, J. High Energy Phys. 10 (2003) 046.
[64] A. Denner, S. Dittmaier, M. Roth, and D. Wackeroth, Nucl. Phys. **B560**, 33 (1999).
[65] A. Denner, S. Dittmaier, M. Roth, and L. H. Wieders, Nucl. Phys. **B724**, 247 (2005).
[66] A. Denner and S. Dittmaier, Nucl. Phys. B, Proc. Suppl. **160**, 22 (2006).
[67] C. Oleari and D. Zeppenfeld, Phys. Rev. D **69**, 093004 (2004).
[68] N. Kauer and D. Zeppenfeld, Phys. Rev. D **65**, 014021 (2001).
[69] S. Catani, Y. L. Dokshitser, and B. R. Webber, Phys. Lett. B **285**, 291 (1992).
[70] S. Catani, Y. L. Dokshitser, and B. R. Webber, Nucl. Phys. **B406**, 187 (1993).
[71] S. D. Ellis and D. E. Soper, Phys. Rev. D **48**, 3160 (1993).
[72] B. Jäger, C. Oleari, and D. Zeppenfeld, J. High Energy Phys. 07 (2006) 015.
[73] B. Jäger, C. Oleari, and D. Zeppenfeld, Phys. Rev. D **73**, 113006 (2006).
[74] G. Bozzi, B. Jäger, C. Oleari, and D. Zeppenfeld, Phys. Rev. D **75**, 073004 (2007).
[75] M. Ciccolini, A. Denner, and S. Dittmaier, Phys. Rev. D **77**, 013002 (2008).
[76] C. Weiser, CMS Note 2006/014.
[77] R. Malhotra, arXiv:hep-ph/0611380.
[78] D. L. Rainwater, R. Szalapski, and D. Zeppenfeld, Phys. Rev. D **54**, 6680 (1996).
[79] D. L. Rainwater, arXiv:hep-ph/9908378.